THE JOURNAL OF PHYSICAL CHEMISTRY C
A JOURNAL OF THE AMERICAN CHEMICAL SOCIETY

pubs.acs.org/JPCC

Article

Development of the ReaxFF Reactive Force Field for Cu/Si Systems with Application to Copper Cluster Formation during Cu Diffusion Inside Silicon

Kamyar Akbari Roshan, Mahdi Khajeh Talkhoncheh, Jonathan E. Mueller, William A. Goddard III, and Adri C. T. van Duin*

Cite This: J. Phys. Chem. C 2021, 125, 19455−19466

Read Online

ACCESS | Metrics & More | Article Recommendations | Supporting Information

ABSTRACT: Transition-metal impurities such as nickel, copper, and iron in solid-state materials like silicon have a significant impact on the electrical performance of integrated circuits and solar cells. To study the impact of copper impurities inside bulk silicon on the electrical properties of the material, one needs to understand the configurational space of copper atoms incorporated inside the silicon lattice. In this work, we developed a ReaxFF reactive force field and used it to perform molecular dynamics simulations on models with up to 762 atoms to study the various configurations of individual and crystalline clusters of copper atoms inside bulk silicon by examining copper's diffusional behavior in silicon. The ReaxFF Cu/Si parameter set was developed by training against density functional theory (DFT) data, including the energy barrier for an individual Cu atom traveling inside a silicon lattice. We found that the diffusion of copper atoms is dependent on temperature. Moreover, we show that individual copper atoms start to form clusters inside bulk silicon at temperatures above 500 K. Our simulation results provide a comprehensive understanding of the effects of temperature and copper concentration on the formation of copper clusters inside a silicon lattice. Finally, the stress−strain relationship of Cu/Si compounds under uniaxial tensile loading has been obtained. Our results indicate a decrease in the elastic modulus with increasing Cu-impurity concentration. We observe spontaneous microcracking of the Si during the stress−strain tests as a consequence of the formation of a small Cu cluster adjacent to the Si surface.

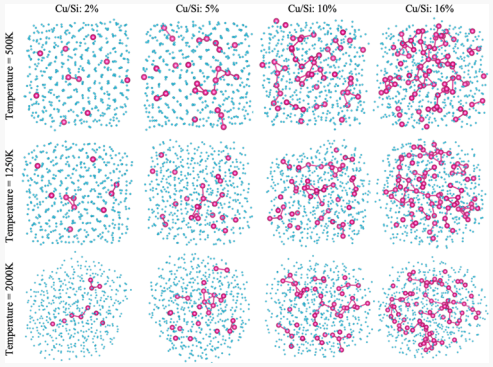

1. INTRODUCTION

The control of impurity contamination in the manufacturing of semiconductor devices has been identified as a critical issue due to their severe impact on the performance of microelectronics.[1] Metallic impurities can be introduced during crystal formation or the fabrication process.[2−4] It has been reported that the 3d transition-metal impurities like Mn, Fe, Co, Ni, and Cu in silica and silicon compounds induce a variety of chemical activities contributing to the alterations in device performance.[5] Nowadays, due to copper's lower bulk resistivity and high activation energy compared to aluminum, copper is considered a suitable alternative for Al in the design of ultra-large-scale integration (ULSI) devices.[6] However, copper has a faster diffusion mechanism in silicon/silica structures in comparison to the other 3d metals, making it capable of quickly migrating over the whole silicon structure within only a few hours, which results in reliability issues.[7] Besides, copper has a high interstitial solubility at high temperatures.[8] The combination of high diffusivity and having a steeply decaying solubility with temperature generates a high driving force for copper precipitation upon cooling. The fast diffusion and clustering of copper ions in dielectric materials play a crucial role in optimizing the performance of microelectronics,[9−12] photonics,[9,13] and electrochemical metallization cells.[14] The copper concentrations in bulk silicon crystals are negligible, as previously reported for iron and nickel.[15,16] However, due to its higher electronegativity compared to that of silicon,[16−18] copper can quickly precipitate on clean silicon wafer surfaces during any wet chemical process.[19−21] Therefore, it is critical to minimize the copper impurity content in chemicals used in device-production lines. Obtaining a more profound knowledge of the underlying molecular rearrangements during the diffusion process is an important step toward fully understanding the evolution of cluster structures. This knowledge can eventually help us to overcome the disadvantage of copper contaminations for interconnected technology.

The molecular dynamics (MD) simulation technique is a suitable method for evaluating mechanical properties, the chemistry of Cu diffusion, and its dissolution inside the silicon

Received: May 11, 2021
Revised: August 13, 2021
Published: August 30, 2021

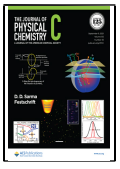

https://doi.org/10.1021/acs.jpcc.1c04178
J. Phys. Chem. C 2021, 125, 19455−19466

structure. MD simulations are capable of providing essential structural information about the system, which can be utilized in further analysis of the electronic properties of the material. Plus, the findings of this study can be leveraged by utilizing machine learning implementations to predict certain electromechanical properties of Cu/Si compounds based on their atomistic structures. Among various MD methods, the ReaxFF family of reactive force fields[22,23] is a powerful tool, available for a wide range of materials, including organic−inorganic,[24−31] organic−metal,[32−34] and metal−metal[35,36] hybrid materials. ReaxFF has been utilized broadly to investigate complicated combustion phenomena,[37−39] interphase chemistry,[40] and mechanical properties of various materials[41] and catalysts.[42] Recently, several systems, including both silica compounds and metals, have been investigated.[5,43,44] Urata et al. studied the interaction between metal copper and amorphous silica (a-SiO_2) as a primitive metal/oxide interaction by using ReaxFF to understand the intrinsic role of an oxidized metal layer on the adhesion between a metal and an oxide glass.[45] In another study, the research carried out by Shirai et al. simulated the fast diffusion of Cu using first-principles calculations.[7] The simulations clearly demonstrated the migration of copper atoms between adjacent cells, and the diffusion constants based on the Arrhenius equation agree with the experimental data. Nonoda et al. investigated the stability of Fe, Cu, and Ni atoms gettering in the large-scale integrated process near the (001) Si surface by performing density functional theory (DFT) calculations.[44] They obtained the formation energy of Fe, Cu, and Ni atoms at the interstitial tetrahedral (T)-site in each atomic layer of Si supercell. It is worth mentioning that during Cu diffusion, crystalline silicon (c-Si) undergoes volumetric expansion, leading to crack nucleation and growth. Cu cluster formation in various sizes is an energetically favorable process that occurs during Cu diffusion inside the Si lattice compared to isolated ions.[14] This indicates that the formation of metallic clusters does not require overcoming a nucleation barrier if the process involves long time scales that allow the silica atoms to relax around the Cu cluster. Moreover, the stability of a copper cluster in silicate and the underlying mechanism of the reaction of a switching cell on a copper electrode has been studied by Guzman et al.[14] Recent transmission electron microscopy (TEM) studies have revealed the atomistic mechanism and dynamics of Cu diffusion inside c-Si.[6] The stress analysis of metal transport in Si lattice during diffusion processes has also been a subject of research. Ostadhossein et al. carried out ReaxFF-based MD simulations to examine lithium diffusion dynamics in silicon nanowires at the atomic scale during the lithiation process.[41] Their stress analysis has shown that lithiation induces compressive stress, causing retardation or even stagnation of the reaction front, also in good agreement with TEM observations.

Although several studies have reported the fast diffusion of copper in silicon,[7] the underlying mechanism of its rapid diffusion remains unclear. In addition, there are limited amounts of studies investigating copper clustering mechanisms inside silicon. In the present work, we developed the Cu/Si force field parameters describing Cu and Si atom's interactions during Cu diffusion and clustering in Si. We compared the migration barriers of Cu in a-Si obtained by ReaxFF with those obtained by DFT calculations to validate the Cu/Si ReaxFF force field. Although we do not directly analyze the electrical properties of the Cu/Si system in this article, we present a method to generate structural inputs for further electrical analysis of this system by studying various configurations that copper atoms incorporate inside the silicon lattice. To this end, we aimed to elaborate a new computational study to atomistically model different arrangements of individual copper atoms in bulk silicon under various conditions such as temperature and the level of Cu contamination. Utilizing reactive force fields enables us to simulate bond formation/breakage along with the dynamics of large molecular systems. In this work, we studied the dependence of Cu crystallization on the contamination level, as well as environmental conditions such as temperature. Finally, the mechanical properties of the Si lattice following Cu diffusion have been investigated. Our results demonstrate the decisive role of Cu atom migration inside pristine Si, which leads to microcrack propagation.

2. METHODS

2.1. Atomistic Scale ReaxFF Simulations. The ReaxFF reactive force field method is a bond order (BO)-based empirical potential that can simulate reactive events by allowing bond formation and bond breakage during molecular dynamics simulation of chemically reactive systems.[46,47] Similar to many nonreactive MD models, ReaxFF consists of two sets of terms: bonded and nonbonded (van der Waals and electrostatic interactions). However, ReaxFF allows bond formation and dissociation and hence has significantly different bonded terms compared to those in classical potentials. ReaxFF uses a bond order−bond distance relation[37] in conjunction with the bond order−bond energy relation, enabling it to properly simulate the smooth formation and dissociation of bonds. All of the connectivity-dependent terms such as bond, angle, and torsion terms are made bond-order-dependent so that their contribution will diminish if the bond breaks. However, nonbonded interactions such as van der Waals and Coulomb are calculated between every pair of atoms irrespective of their connectivity. Though the nonbonded interactions are not bond-order-dependent, they are highly dependent on the distance of the atom pairs. Therefore, these contributions need to be updated at each step of the simulation. ReaxFF calculates atomic charges by using the electronegativity equalization method.[48] Additionally, to eliminate discontinuities in the nonbonded interaction energies and reduce the range of the Coulomb interactions, a seventh-order Taper function is employed.[49,50] The Taper function ensures that all nonbonded terms, together with their first, second, and third derivatives, go to zero at the nonbonded cutoff distance, which is typically picked to be 10 Å.[51] In short, ReaxFF uses the following equation to find the energy of the system

$$E_{system} = E_{bond} + E_{over} + E_{under} + E_{lp} + E_{val} + E_{tor} + E_{vdWaals} + E_{Coulomb} + E_{trip} \quad (1)$$

where E_{bond}, E_{over}, E_{under}, E_{lp}, E_{val}, E_{tor}, $E_{vdWaals}$, $E_{Coulomb}$, and E_{trip} represent bond energy, overcoordination energy penalty, undercoordination stability, lone-pair energy, valence angle energy, torsion angle energy, van der Waals energy, Coulomb, and triple bond stabilization energies, respectively. A more detailed description can be found in previous ReaxFF-related articles.[52−55] After training against energetic and conformational data from quantum mechanics (QM) calculations, ReaxFF can provide atomistic descriptions of many complex chemical reactions, including the interactions between Cu and Si atoms, as presented here.

https://doi.org/10.1021/acs.jpcc.1c04178
J. Phys. Chem. C 2021, 125, 19455−19466

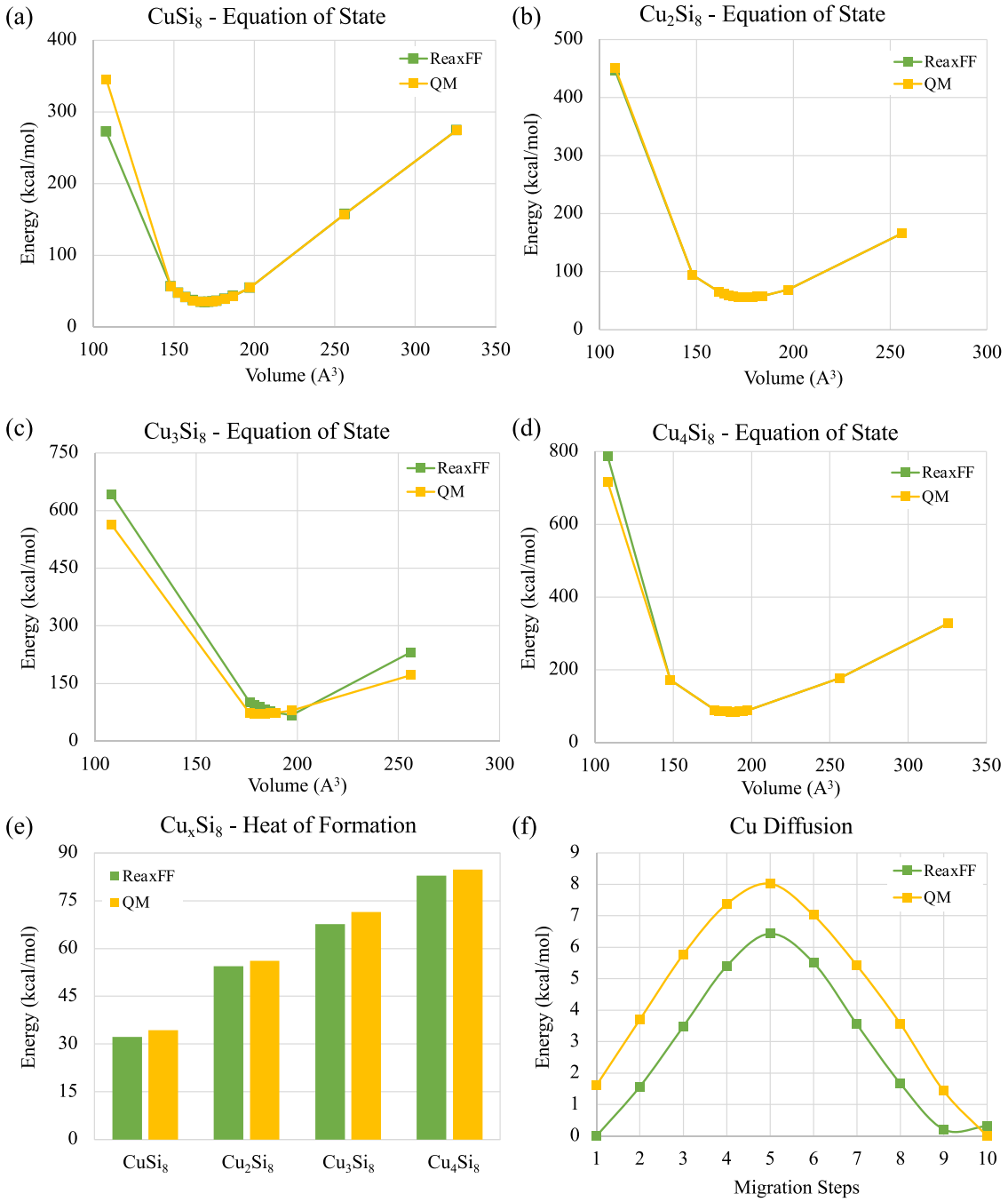

Figure 1. (a–d) Birch–Murnaghan equation of state for four different Cu_xSi_8 species ($CuSi_8$, Cu_2Si_8, Cu_3Si_8, Cu_4Si_8) using QM and ReaxFF methods. (e) Heat of formation for Cu_xSi_8 species using QM and ReaxFF methods. (f) Copper migration energy barrier to the nearby adjacent vacancy site in silicon lattice calculated by ReaxFF and QM showing that ReaxFF can properly reproduce QM results.

2.2. Force Field Development. The quality of a molecular dynamics simulation depends on the accuracy of the force field parameters; therefore, these parameters need to be trained against available experimental or quantum mechanical-based data.[56,57] To initiate the simulation on relatively large-scale systems (≫1000 atoms) to study the chemistry of Cu diffusion inside the Si system, we have developed a-Si/Cu reactive force field parameter sets to include the descriptions of Cu and Si atom interactions during dissolution and clustering. These parameters have been trained against density functional theory (DFT) data, including equation of state (EOS), Cu diffusion data, and heats of formation of crystalline phases and molecules. The optimization of the parameters was performed via a successive one-parameter search technique to minimize the sum of error values

$$\text{error} = \sum_{i}^{n} [x_{i,\text{QM}} - x_{i,\text{Reaxff}}/\sigma_i] \quad (2)$$

where $x_{i,\text{QM}}$ is the QM value, $x_{i,\text{Reaxff}}$ is the ReaxFF calculated value, and σ_i is the weight assigned to the data point, i.[58] Generally, we train our ReaxFF force field at effectively 0 K temperature. However, since we apply various mechanical strains to the system during force field training (volume expansion and compression of the system), we can confidently

https://doi.org/10.1021/acs.jpcc.1c04178
J. Phys. Chem. C 2021, 125, 19455–19466

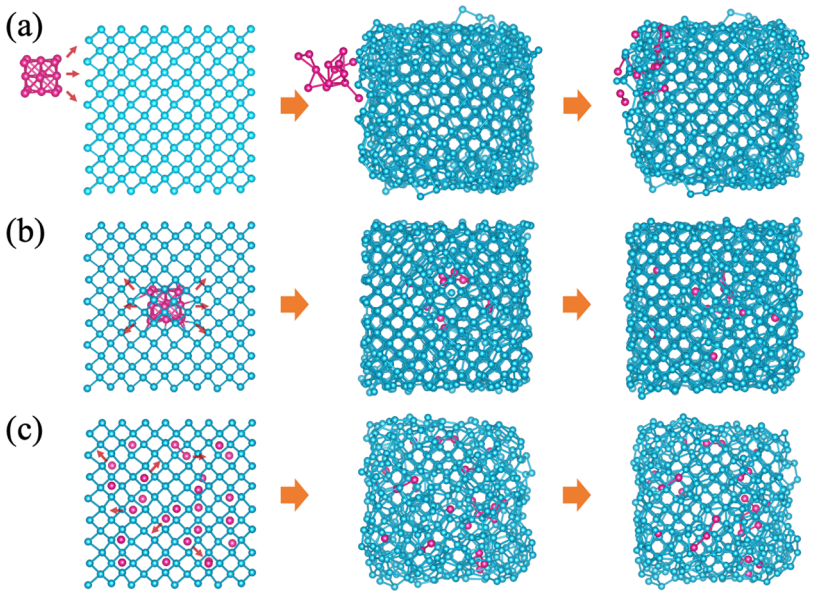

Figure 2. Snapshots of the Cu (pink spheres) and Si (light blue spheres) structures at the initiation, halfway, and end of the MD simulation for three configurations: (a) 14-atom Cu cluster diffuses into the 512-atom Si supercell, (b) 14-atom Cu cluster diffuses inside the 512-atom Si supercell, and (c) individual Cu atoms diffuse inside the 512-atom Si supercell.

claim that the force field can reliably simulate the behavior of the system in nonzero temperature ranges.[52]

To parameterize the ReaxFF equation-of-state (EOS) data, we carried out QM calculations for the EOS in various molecular species, such as $CuSi_8$, Cu_2Si_8, Cu_3Si_8, and Cu_4Si_8. Figure 1 compares ReaxFF and QM results for Birch−Murnaghan isothermal equations of state (a−e) and copper diffusion barrier (f). In each case, we constructed ground-state geometries through complete geometry optimization. The Birch−Murnaghan equation-of-state calculation[59] was performed on crystalline Cu_xSi_y (various space groups). We carried out periodic QM calculations based on density functional theory (DFT). The Vienna ab initio simulation package (VASP) was used to solve the Kohn−Sham equations with periodic boundary conditions and a plane-wave basis set.[60,61] We applied Blöchl's all-electron frozen core projector-augmented wave (PAW) method,[62] and electron exchange and correlation are treated within the generalized gradient approximation (GGA) of Perdew−Burke−Ernzerhof (PBE).[63] We applied compression and expansion with respect to the equilibrium volume of the crystal to calculate QM energies at different volume states. Next, during force field optimization, the energy values corresponding to each volume calculated by ReaxFF are compared with the QM data. To obtain a reliable force field, the ReaxFF force field parameters were trained against quantum mechanics data. Since the results from ReaxFF MD simulations are in good agreement with DFT data (within 10% error), we can argue that the developed force field replicates the DFT data with acceptable accuracy. Previously reported direct comparisons between ReaxFF and DFT-based confirm that ReaxFF potentials trained against DFT calculations of static structures are able to reproduce the trends observed during DFT-based MD simulations.[64]

Figure 1a−d shows the EOS of the Cu_xSi_y crystal as predicted by ReaxFF and QM. In addition, the heat of formations for the Cu_xSi_8 species were also utilized in the force field development by using the following relation (Figure 1e)

$$\Delta E = E_{Cu_xSi_y} - xE_{Cu} - yE_{Si} \quad (3)$$

where $E_{Cu_xSi_y}$ is the total energy of the Cu−Si system, x and y are the atomic fraction of copper and silicon, respectively, and E_{Cu} and E_{Si} are the energies per atom for Cu and silicon, respectively. The formation energies are in reasonable agreement with the values obtained from DFT, indicating that the developed force field can simulate reliable thermodynamic behavior for the Cu/Si systems. Furthermore, we trained our force field for Cu atom migration inside the Si lattice. ReaxFF parameters were fitted against QM results for the individual Cu atom migration through the Si unit cell, which can be seen in Figure 1f. Overall, ReaxFF energy descriptions are in good agreement with the QM data, which establishes the capability of the force field to describe the chemistry of copper silicon interactions. The force field parameters are provided in the Supporting Information. In this study, the ReaxFF force field utilizes a significant number of equations-of-state (EOS) data for Si, Cu, and Cu/Si compounds with different Cu concentrations during training. Thus, this training set is diverse enough so that the trained force field should reliably reproduce QM results for the Cu/Si systems. Since we have not directly included any loop, chain, or diamond morphologies of Cu atoms in force field training, it would be an extremely helpful future work to take the structures extracted from molecular dynamics simulation results and return back to DFT calculations to judge how well the force field predicts the QM results. Additionally, it would also be possible to explicitly train the force field against the Cu/Si compounds with Cu loop, chain, and diamond structures to create a version of the force field specifically designed to describe these types of structures.

2.3. Simulation Methodology. We employed our Cu−Si force field to study Cu diffusion and dissolution inside silicon lattice. Initial geometries were constructed in three configurations: (1) placing a 14-atom Cu crystal outside of Si lattice with 512 atoms, (2) placing a 14-atom Cu crystal inside of Si lattice with 512 atoms, and (3) randomly dispersing individual Cu atoms at the given concentrations in a silicon lattice phase composed of 512 atoms (Figure 2). These geometries were relaxed using a conjugate gradient minimization scheme. We performed an equilibration of the box in three stages: the first

https://doi.org/10.1021/acs.jpcc.1c04178
J. Phys. Chem. C 2021, 125, 19455−19466

stage is performed at 50 K for 50 ps to eliminate any hot spots in the initial geometry. Next, the temperature is increased from 50 K to various temperatures (i.e., 300, 500, 700, 1000, 1200, 1500, 1700, and 2000 K) at a rate of 2.5 K ps^{-1} in NVT (constant volume, temperature) ensemble. Finally, in the third stage, the box is equilibrated at a target temperature of 200 ps. Temperature and pressure were regulated using the Berendsen thermostat and barostat,[65] respectively. These three stages were performed using the NVT ensemble with a temperature relaxation time of 100 fs at 1 atmosphere and with a pressure relaxation time of 100 ps. Periodic boundary conditions were employed in all three directions, and an MD time step of 0.25 fs was used for all of the simulations in this study.

3. RESULTS AND DISCUSSION

The three configurations studied in this work are shown in Figure 2. In each configuration, the initial, halfway, and final snapshots of the Cu/Si system are shown in the first, middle, and final columns, respectively. In the first configuration, a Cu cluster consisting of 14 Cu atoms is initially placed adjacent to the silicon supercell. As indicated in Figure 2a, immediately after starting the MD simulation, the Cu cluster starts to deform and diffuses into the Si supercell at a temperature below its melting point, which is due to the high surface-to-volume ratio of the Cu cluster.[66,67] In the second configuration, the same Cu cluster as in the previous configuration is placed inside the Si supercell. By running the MD simulation on this structure, the Cu cluster diffuses inside the Si cluster through the interstitial sites. In the final configuration, individual Cu atoms are randomly placed within the Si interstitial sites. When the individual Cu atoms diffuse inside the Si supercell, they begin to form Cu clusters. This phenomenon is investigated throughout this paper.

3.1. Cu Cluster Diffusion Starting Outside the Silicon Lattice. For the first stage of our work, the simulations are done in canonical ensemble (NVT) at different temperatures ranging from 300 to 1000 K. The Cu concentration is about 2.7% (14−512). We observe that the Cu atoms start to diffuse into the Si cluster instantly at the beginning of the MD simulation. The motion of Cu atoms is traced by their mean-squared displacement (MSD), and it is used to calculate the diffusion coefficient. Figure 3 shows the MSD data for the Cu atoms migrating inside silicon lattice as a function of simulation time

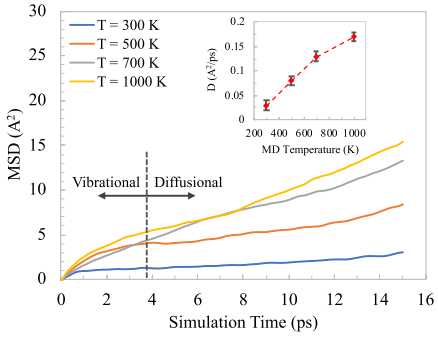

Figure 3. Mean-squared displacement of Cu atoms as a function of simulation time running under four different temperatures from 300 to 1000 K. The initial nonlinear increase in the MSD belongs to the vibrational motions, while the linear section indicates the diffusional motion of Cu atoms through the interstitial sites of Si lattice. The inset shows the diffusion coefficient of copper atoms as a function of temperature.

for four different MD temperatures (300, 500, 700, and 1000 K). The diffusion coefficient for each case is calculated by using eq 4[68]

$$D_i = \lim_{t\to 0} \frac{\langle [r(t) - r(0)]^2 \rangle_i}{6t} = \frac{1}{6}\frac{\mathrm{d(MSD)}}{\mathrm{d}t} \tag{4}$$

where D_i represents the diffusion coefficient, and it is obtained from the slope of the MSD curves (Figure 3). It is known from the calculations that temperature increase should lead to more rapid Cu atom diffusion into the Si lattice. At the beginning of the simulation, the MSD curve nonlinearly increases and plateaus, which indicates that the particles are confined. In other words, the particles are stationary, vibrating at the first 5 ps of the simulation. The rest of the MSD plot could be considered as the diffusional behavior in which the MSD becomes more linear. The inset of Figure 3 shows the diffusion coefficient of Cu atoms as a function of MD temperature. The data indicates that there is an exponential relation between the diffusion coefficient and MD temperature, which is in agreement with the following Arrhenius equation[69]

$$D(T) = D_0 \exp\left(-\frac{E_a}{kT}\right) \tag{5}$$

In the equation above, $D(T)$ is the temperature-dependent diffusion coefficient, D_0 is the pre-exponential factor of maximum diffusion at infinite temperature, E_a is the activation energy for diffusion, k is the Boltzmann constant, and T is the temperature. Since the experimentally observed pre-exponential factor (D_0) in the diffusion coefficient has approximately the same value for all of the 3d transition-metal (TM) impurities in silicon, the significant differences of diffusivity among these elements come primarily from the difference in the diffusion barrier (E_a).[5,70] The resulting pre-exponential factor for Cu atoms inside silicon is 3.6×10^{-7} (cm^2 s^{-1}), which is in agreement with the experimental results.[5,70] The diffusion coefficients are calculated using the mean-squared displacement of Cu and Si atoms as a function of simulation time at different temperatures. Increasing the MD temperature leads to an increase in the diffusion coefficient; thus, we can argue that the diffusion is temperature-dependent. The underlying mechanism behind this phenomenon should be directed to the electronic origin of the elements, which makes the difference of the diffusion coefficient between the early 3d TM and the late 3d TM impurities in silicon almost 1 order of magnitude.[5,71]

To examine the accuracy of the ReaxFF method and to obtain a better insight into the Cu diffusion, we investigated the energy barriers for the diffusion of a single Cu atom through a diamond cubic supercell of 64 Si atoms, corresponding to a $2 \times 2 \times 2$ multiple of the 8-atom diamond cubic cell. Here, we use a bond-restraint approach to find the minimum energy pathways on the potential energy surface between two sites for Cu insertion that represents stable local energy minima. To explore the Cu migration pathways between two equilibrium neighboring sites of the Cu atom, a penalty potential function is added to the ReaxFF energy to maintain the distance between two adjacent sites using eq 6

$$E_{\mathrm{restraint}} = f_1(1 - e^{f_2(r_0 - r_{ij})^2}) \tag{6}$$

In this equation, f_1 and f_2 are constants; during each MD step, the value of the distance between two sites r_{ij} is modified to sample the pathway between two local minima separated by the initial distance r_0. For the case of a single Cu atom in c-Si, the

https://doi.org/10.1021/acs.jpcc.1c04178
J. Phys. Chem. C 2021, 125, 19455−19466

thermodynamically favorable site for Cu atom insertion is the tetrahedral (T_d) interstitial. The Cu diffusion path consists of the Cu migration between two adjacent T_d interstitial sites passing through the hexagonal (Hex) site. A comparison of the energy landscape along the diffusion pathway obtained by DFT and ReaxFF is shown in Figure 4. The initial, saddle-point, and final state of the Cu atom are also indicated throughout this transition. The energy barrier height obtained from our MD simulation is about 1.1 eV, which is in reasonable agreement with the DFT result (1.5 eV). The difference between the calculated energy barriers in Figures 1f and 4 is due to the variation in Si density in the structures. The 8-atom Si unit cell studied in Figure 1f has a higher cell volume (greater lattice parameters) in comparison with the 64-atom Si supercell (Figure 4), which leads to a lower density of Si atoms (2.43 g cm^{-3} for $CuSi_8$ vs 2.85 g cm^{-3} for $CuSi_{64}$) and thus an easier Cu migration inside the Si lattice.

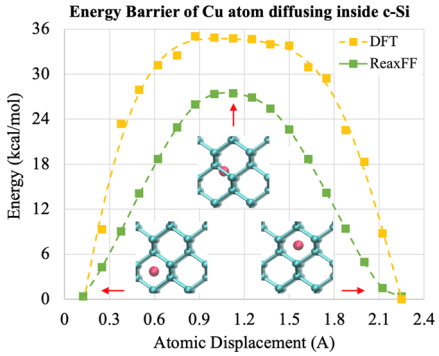

Figure 4. Energy landscape for the diffusion of an individual Cu atom in c-Si from one equilibrium T_d site to an adjacent one through the hexagonal configuration calculated by DFT (yellow) and ReaxFF (green). The light blue spheres represent Si atoms and the pink spheres represent the Cu atom in its initial, saddle-point, and target (final) configuration.

3.2. Copper Cluster Diffusion Starting Inside the Silicon Lattice. In the following section, we studied the diffusional behavior of copper atoms inside bulk silicon. The initial 14-atom Cu cluster is placed within the same silicon cluster similar to the last section (Figure 2b). MD simulations are performed at temperatures ranging from 1000 to 1700 K in the NVT ensemble. To trace the motion of the system, MSD data for Cu (a) and Si (b) atoms are plotted as a function of simulation time for four different temperatures (1000, 1200, 1500, and 1700 K) in Figure 5. The MSD plot shows that Cu diffusion at lower temperatures is not considerable. This means that higher temperatures (above 1000 K) are required to trigger the Cu diffusion. On the other hand, silicon atoms do not show any diffusion compared to the Cu atoms, indicating that the Si lattice keeps its crystalline structure throughout the simulation.

In line with the MSD analysis, we looked at the radial distribution function (RDF) of Cu atoms inside Si. The integration of the RDF for Cu atoms as a function of radius for the MD simulation at 1500 K is shown in Figure 6, which shows the number of Cu atoms within the specific integration range. Each line of data indicates the integral at a certain time during the MD simulation moving from the start (darker) to the end (lighter). Since Int $g(r)$ illustrates the coordination number of the atoms, it can provide an insight into the number of neighboring atoms as a function of time. At the beginning of the simulation (the darkest line), Cu atoms are keeping their crystalline form. Over time, the Cu cluster loses its crystalline structure and diffuses into the Si. To look at the number of neighboring Cu atoms within a radius of 3.2 A, we can simply draw a vertical line in Figure 6a at a radius of 3.2 A and plot the integral of RDF as a function of simulation time. As shown in Figure 6b, the number of neighboring atoms starts to decrease as the Cu atoms diffuse into the Si throughout the simulation. The inset of Figure 6b shows the RDF of Cu−Cu, Si−Si, and Cu−Si atom pairs as a function of radius. It is noteworthy that $g(r)$ peaks at approximately 2.3 and 2.7 A for Si and Cu atoms, respectively. These peaks correspond to the Cu−Cu and Si−Si bond lengths, which strongly agree with the experimental data,[72−74] supporting the quality of our Cu/Si force field.

3.3. Copper Ion Diffusion and Clustering Starting Inside the Silicon Lattice. For the final configuration of the Cu/Si system, we looked at individual Cu atoms randomly placed inside Si sites within the Si lattice. The clustering of Cu atoms inside the Si crystal is investigated by running NVT molecular dynamic simulations at different temperatures and Cu concentrations. The snapshots of the Cu migration inside the Si structure during simulations under three temperature regimes (500, 1250, 2000 K) with four initial levels of copper concentrations (2, 5, 10, and 16%) are shown in Figure 7. For these experiments, the MD temperature is fixed at 500, 750, 1000, 1250, 1500, 1750, and 2000 K, and the Cu concentration is set to 2, 3, 5, 10, 16, 30, and 49%. The simulation time step is set to 0.25 fs, making a cumulative simulation time of 725 ps. An interesting behavior of Cu atoms observed during the simulations is that they start to approach each other and form

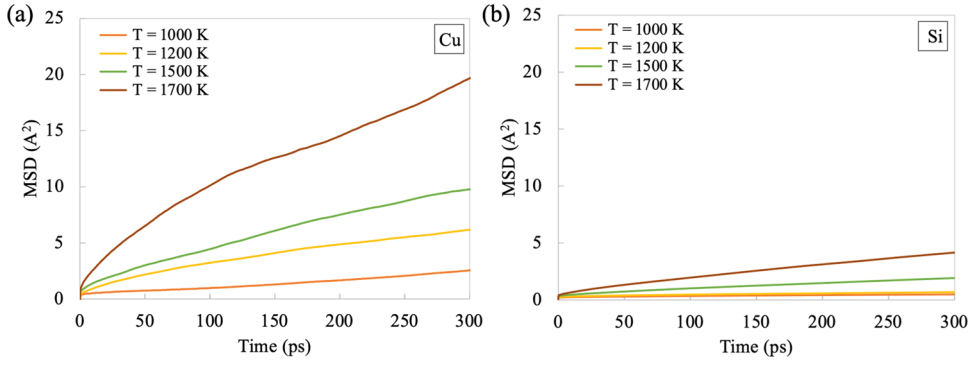

Figure 5. Mean-squared displacement of Cu (a) and Si (b) atoms as a function of simulation time at different temperatures ranging between 1000 and 1700 K.

https://doi.org/10.1021/acs.jpcc.1c04178
J. Phys. Chem. C 2021, 125, 19455−19466

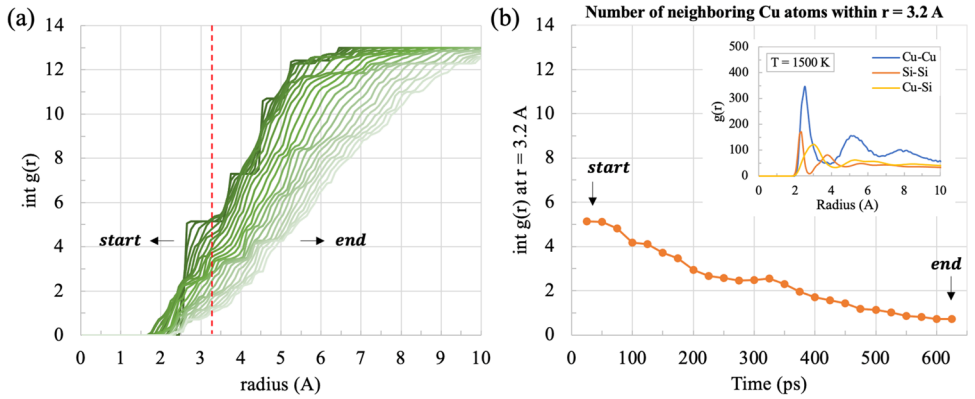

Figure 6. (a) Integral of radial distribution function for Cu atoms as a function of radius for the MD simulation at 1500 K. (b) Number of neighboring copper atoms within 3.2 A as a function of simulation time. The inset shows the radial distribution function for Cu−Cu, Si−Si, and Cu−Si atom pairs as a function of radius.

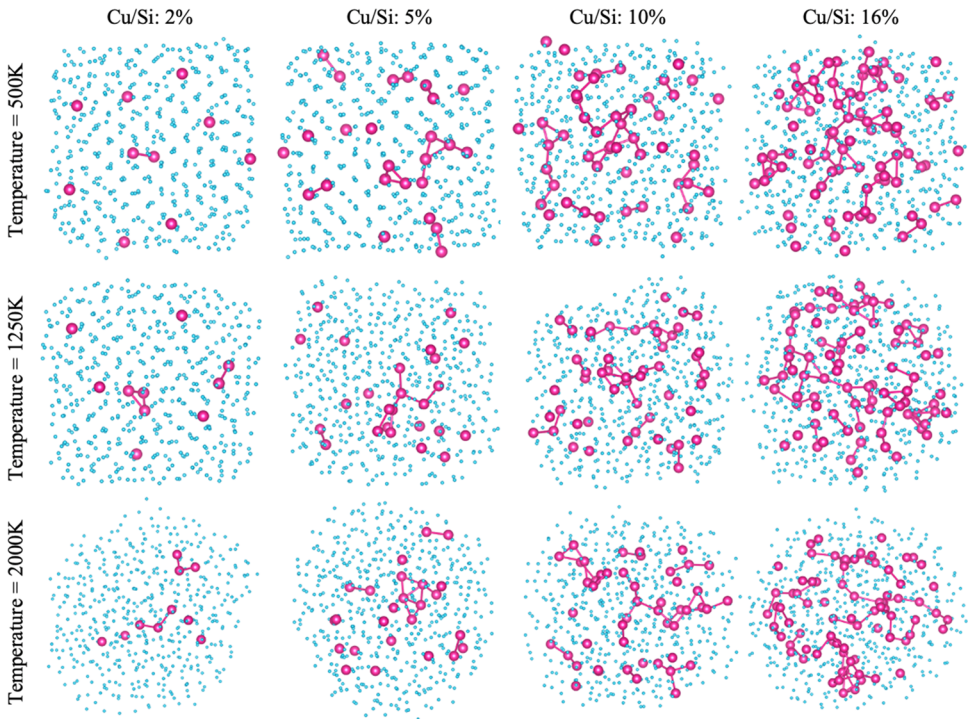

Figure 7. Snapshots of the Cu (pink spheres) and Si (light blue spheres) structures while running the MD simulation under three temperature regimes (500, 1250, 2000 K) with four initial levels of copper concentrations (2, 5, 10, and 16%).

bonds with the surrounding copper atoms, which plays the main role in the formation of copper crystals during the simulation. As indicated in Figure 7, Cu clustering is strongly related to the Cu concentration. Bigger clusters and chain structures of Cu atoms form by increasing the Cu concentration. In addition, higher temperature helps with Cu clustering since the Cu atoms need a starting momentum to overcome the energy barrier and diffuse through the silicon lattice. However, it can be observed from Figure 7 that Cu clustering is decreased at the highest temperature. This is due to the fact that very high temperatures make the kinetic energy of Cu atoms high enough to prevent them from staying at one place and maintain the existing bonds with the surrounding Cu atoms. In addition, higher temperatures lead to thermal stresses on the system and breaking the formed bond in the Cu cluster.

3.4. Copper Clustering Analysis. Due to its direct impact on device performance, an important feature of the Cu clusters formed during the simulation is their structural properties. The overall electrical conductivity of the system is significantly altered by the existence of chain, loop, or diamond-shaped Cu clusters. Therefore, we analyzed the structure of the Cu/Si configurations by using the connected-component clustering (CCC) algorithm.[75−78] Using CCC, for each simulation at a particular time and a specific Cu concentration, we can import the Cartesian coordinates of Cu atoms inside the structure, calculate the Euclidian distance for each copper atom pair, and classify them into separate clusters as a function of simulation time. This classification is based on the bonds created between individual copper atoms, which can be extended to any other element of interest. Since the optimized bond length between the Cu−Cu atom pair is approximately 2.7 A, the maximum bond length used for this classification is 3 A. Following this approach, we can obtain useful structural information about our system, such as the size and geometry of the Cu clusters during

https://doi.org/10.1021/acs.jpcc.1c04178
J. Phys. Chem. C 2021, 125, 19455−19466

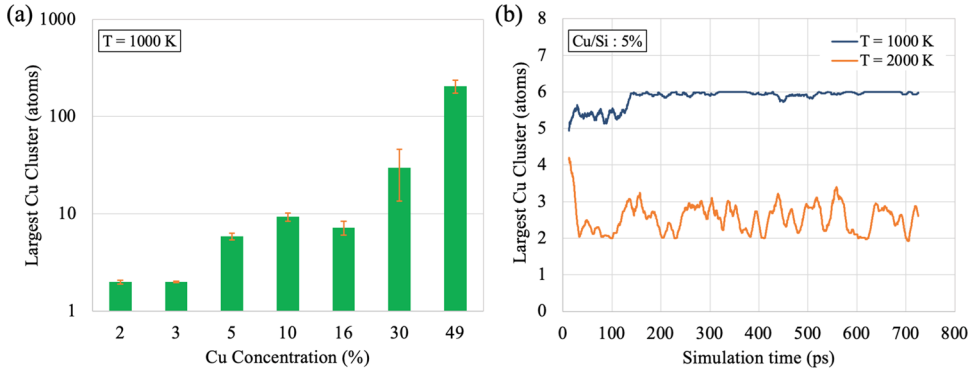

Figure 8. (a) Average size of the largest Cu cluster formed during the MD simulation in the NVT ensemble at 1000 K as a function of the initial Cu concentration. (b) Average size of the largest Cu cluster formed during the MD simulation in NVT ensemble at 1000 and 2000 K as a function of simulation time.

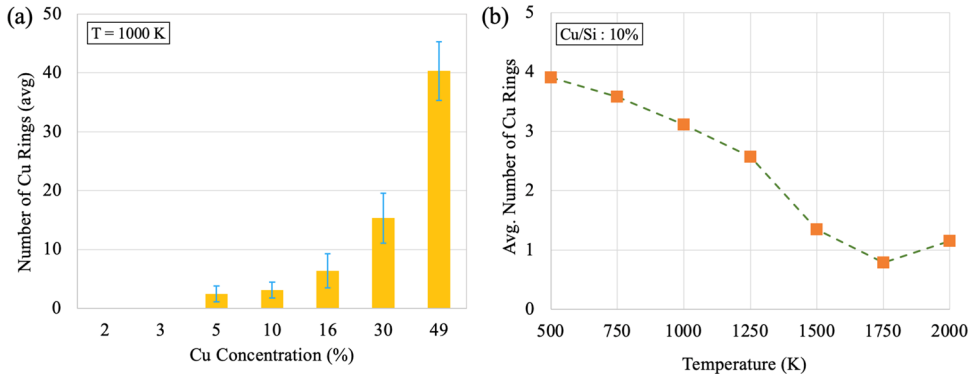

Figure 9. (a) Average number of Cu 3-atom rings formed during the MD simulation in NVT ensemble at 1000 K as a function of the initial Cu concentration. (b) Average number of Cu 3-atom rings formed during the MD simulation in NVT ensemble at a Cu concentration of 10% as a function of MD temperature.

the simulation, the number of Cu clusters within the Si crystal, RDF of Cu atoms, and the number of 3-membered Cu rings within the structure. Three-membered Cu rings are the simplest form of Cu clusters that can easily attract an additional Cu atom and form a 4-membered Cu diamond.

The average size of the largest Cu cluster as a function of Cu concentration for the simulation at 1000 K is shown in Figure 8a. As indicated by the plot, Cu concentration has a direct impact on Cu crystallization. Figure 8b shows the time-trace of the average size of the largest Cu cluster for the simulations at 1000 and 2000 K. As indicated in the figure, at 2000 K, Cu atoms show longer and recurrent movements inside the Si cluster, which is due to their higher kinetic energy. However, at 1000 K, Cu atoms show limited movements, which leads to a smaller change in the size of the largest Cu cluster.

In addition, the CCC algorithm also observes the number of 3-membered Cu rings throughout the simulation (Figure 9a). Based on this plot, the number of Cu rings is directly related to the Cu concentration. As indicated in Figure 9a, Cu concentrations of 3% and below do not produce any Cu rings. However, there is an exponential relation between the number of Cu rings and the Cu concentrations above 5%. Moreover, we see that the number of Cu rings has a reverse relation with the MD temperature. Figure 9b shows the average number of 3-membered Cu rings as a function of temperature. We observed that at lower temperatures, more Cu rings were formed during the simulation, which is in agreement with our previous argument. However, at higher temperatures, due to the higher kinetic energy and rapid movements of Cu atoms through the Si sites, a lower number of 3-membered Cu rings are observed.

Another interesting observation from the analyzed results of the CCC algorithm is the number of Cu clusters during the simulation as a function of Cu concentration. Figure 10 reveals

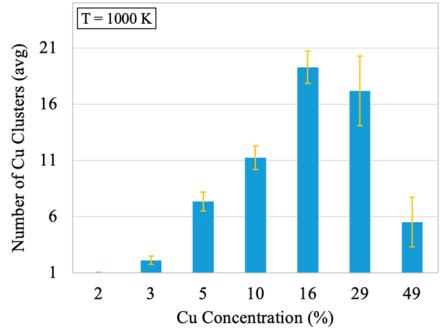

Figure 10. Average number of Cu clusters formed during the MD simulation in NVT ensemble at 1000 K as a function of Cu concentration.

that during the simulation at 1250 K, no Cu clusters of any form are observed at lower Cu concentrations. On the other hand, increased Cu contaminations will usually lead to the formation of a single large Cu cluster. Based on this observation, we can argue that with around 16% initial Cu concentration, the maximum number of Cu clusters can be observed during the simulation at 1000 K. Figure 11 shows the integral of RDF for

https://doi.org/10.1021/acs.jpcc.1c04178
J. Phys. Chem. C 2021, 125, 19455−19466

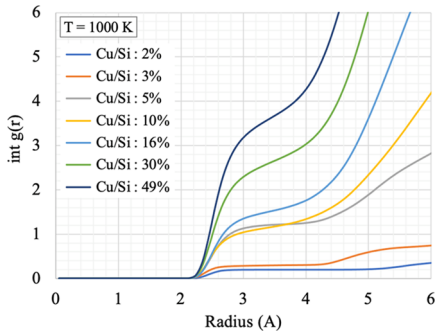

Figure 11. Integral of radial distribution function for Cu atoms as a function of radius at 1000 K.

the Cu−Cu atom pairs inside the Si crystal for different initial Cu concentrations by running the simulation at 1000 K. As expected, the number of neighboring Cu atoms increases by increasing the Cu concentration. An interesting observation from Figure 11 is that there is a slight gap between the number of neighboring atoms for the Cu concentrations of (3%-under) and (5%-above). This observation indicates that concentrations of 5% and above are more likely to form Cu clusters during the simulation.

3.5. Mechanical Properties. To characterize the mechanical behavior of the Cu/Si compounds, we performed MD simulations at room temperature to obtain the stress−strain relationship under uniaxial tensile loading. We considered seven different samples (2, 3, 5, 10, 16, 29, and 49% Cu concentrations) to investigate the effects of Cu contamination on the mechanical properties of the system. Figure 12 shows

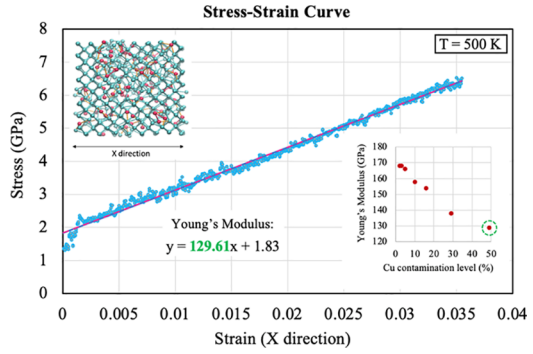

Figure 12. Tensile stress−strain curves at a strain rate of 1 A ns^{-1} during the MD simulation for the sample with a 29% Cu concentration inside the Si lattice at T = 500 K. Young's modulus is calculated using a linear fit to the stress−strain curve. The inset shows Young's modulus as a function of Cu concentration.

tensile stress−strain curves at a strain rate of 1 A ns^{-1} during the 125 ps simulation time for the sample with a 29% Cu concentration inside the Si lattice. Similar trends in the stress−strain curve at other Cu concentrations have been observed in Cu/Si lattice deformation simulations.[45] In general, stress−strain curves exhibit an initial linear region followed by a nonlinear portion. The linear portion of the uniaxial stress−strain curve corresponds to elastic deformation, and the gradient of this part is Young's modulus (YM). Since utilizing the realistic experimental strain rates is highly time-consuming, the models were subjected to strain rates in the range of 10^{-1}−10^{2} A ns^{-1} (Table 1), which is higher than typical experimental tests.[79] Subsequently, Young's modulus is calculated by using linear

Table 1. Young's Modulus as a Function of Strain Rate for a Cu Concentration of 50% Inside Si Lattice at T = 500 K[a]

strain rate (A ns^{-1})	0.5	1	10	100
Young's modulus (GPa)	117.32	129.61	138.96	171.04

[a]Young's modulus is calculated using a linear fit to the stress−strain curve.

regression on the initial linear portion. It is worth mentioning that Young's modulus can be calculated by extrapolation to physically realistic experimental strain rates reported by previous experimental works.[69,80] The calculated result for YM for various compositions of Cu is shown in Table 1, and they are plotted in the inset of Figure 12. The results demonstrate that YM will drop with increasing Cu concentration, which is in good agreement with experimental data.[81] Special attention should be drawn to the decrease in elastic modulus while increasing the level of impurity concentration. In this phenomenon, spontaneous microcracking of the Si matrix occurs during the stress−strain test. Microcrack propagation in the presence of an external load applied on the Si lattice is shown in Figure 13. A small cluster of Cu is formed where the cracking initiates, and as a result, the nearby Si−Si bonds are broken throughout the simulation. Inclusions can also be fracture initiators due to the thermal residual stresses introduced during processing and the intensification of stress in the surroundings of the inclusions that occurs when an external load is applied.

The diffusion of copper atoms into the silica layer is one of the critical problems for ultra-large-scale integration (ULSI) metallization. Although copper concentrations studied in this work are beyond practical values, the findings of this study can be further accompanied by machine learning implementations to predict certain electromechanical properties of Cu/Si compounds. For instance, numerous samples of various environmental conditions, structural parameters, initial concentrations, and electrical conductivity of the system calculated by tight-binding DFT (DFTB) techniques can be given to the AI as an input. In return, AI learns to predict the electrical conductivity given the initial status of the system. DFTB methods offer a handful of advantages, including the ability to analyze larger systems and accessing longer time scales.

4. CONCLUSIONS

In this study, we first developed the ReaxFF reactive force field for Cu/Si systems to describe the diffusion process of Cu impurities inside the Si lattice. The optimized force field was validated with a variety of data comparing the results from ReaxFF and quantum mechanics for Birch−Murnaghan isothermal equations of state and copper diffusion barrier.

We then performed a computational study to model Cu diffusion and incorporation inside the Si lattice in three different configurations. We observed that temperature has a strong impact on the Cu diffusion coefficient. In addition, we observed an increased number of Cu clusters and 3-membered Cu rings with higher levels of Cu concentrations. These simulations find that Cu concentrations of 5% and above are likely to form Cu clusters. We also carried out tensile stress/strain analysis to characterize the mechanical behavior of Cu/Si compounds. Our results demonstrate that Young's modulus drops with increasing Cu concentration, which is in good agreement with experimental data. Furthermore, we observed spontaneous microcracking of the Si matrix in the presence of an external load applied to the Si lattice. We show that this cracking initiates from

https://doi.org/10.1021/acs.jpcc.1c04178
J. Phys. Chem. C 2021, 125, 19455−19466

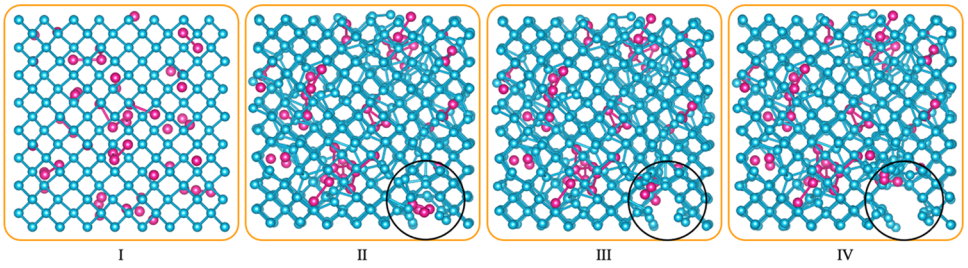

Figure 13. Snapshots of the Cu (pink spheres) and Si (light blue spheres) structures while running the MD simulation, indicating the microcrack propagation when Cu impurities are present in the Si lattice under a stress load.

the formation of a small Cu cluster, which breaks nearby Si−Si bonds during the simulation.

Compared to other currently used experimental and computational methods, ReaxFF provides a powerful tool for multiscale simulations to investigate the mechanical and chemical effects of Cu dissolutions inside Si. These simulations provide new insight into the diffusional behavior of Cu inside Si, which is of fundamental interest and importance in modern electronics and semiconductor technologies. In particular, our study of the mechanical properties of Cu/Si compounds suggests that Cu clusters initiate microcrack formation, which has a significant impact on the electronic response of the material. Furthermore, microcracks may provide critical initiation points for oxidation processes inside the Si matrix. Therefore, the developed ReaxFF reactive force field provides a unique, powerful tool for multiscale simulations to investigate the mechanical and chemical effects of Cu dissolutions inside Si.

■ ASSOCIATED CONTENT

Supporting Information

The Supporting Information is available free of charge at https://pubs.acs.org/doi/10.1021/acs.jpcc.1c04178.

Cu/Si reactive force field parameter sets are developed to include the descriptions of Cu and Si atom interactions during dissolution and clustering; these parameters have been trained against density functional theory data, including equations of state, Cu diffusion data, and heats of formation of crystalline phases and molecules; the optimization of the parameters was performed via a successive one-parameter search technique to minimize the sum of error values (PDF)

■ AUTHOR INFORMATION

Corresponding Author

Adri C. T. van Duin − *Department of Chemical Engineering and Department of Mechanical Engineering, Pennsylvania State University, University Park, Pennsylvania 16802, United States;* orcid.org/0000-0002-3478-4945; Phone: +1-814-863-6277; Email: acv13@engr.psu.edu

Authors

Kamyar Akbari Roshan − *Department of Electrical Engineering, Pennsylvania State University, University Park, Pennsylvania 16802, United States;* orcid.org/0000-0001-8343-0142

Mahdi Khajeh Talkhoncheh − *Department of Chemical Engineering, Pennsylvania State University, University Park, Pennsylvania 16802, United States*

Jonathan E. Mueller − *Materials and Process Simulation Center, California Institute of Technology, Pasadena, California 91125, United States;* Present Address: Volkswagen AG, Berliner Ring 2, 38436 Wolfsburg, Germany

William A. Goddard III − *Materials and Process Simulation Center, California Institute of Technology, Pasadena, California 91125, United States;* orcid.org/0000-0003-0097-5716

Complete contact information is available at: https://pubs.acs.org/10.1021/acs.jpcc.1c04178

Notes

The authors declare no competing financial interest.

■ ACKNOWLEDGMENTS

This work was supported by NSF DMR grant #DMR-1842952. KR, MT and ACTvD acknowledge the support by a grant from the U.S. Army Research Laboratory through the Collaborative Research Alliance (CRA) for Multi-Scale Multidisciplinary Modeling of Electronic Materials (MSME) under Cooperative Agreement No. W911NF- 12-2-0023. Computations for this research were performed on the Pennsylvania State University's Institute for Cyber ScienceAdvanced Cyber Infrastructure (ICS-ACI). W.A.G. and J.E.M. were supported by NSF (CBET-1805022).

■ REFERENCES

(1) Claeys, C.; Simoen, E. *Metal Impurities in Silicon- and Germanium Based Technologies: Origin, Characterization, Control, and Device Impact*; Springer: Heidelberg, 2018.

(2) Harada, K.; Tanaka, H.; Matsubara, J.; Shimanuki, Y.; Furuya, H. Origins of Metal Impurities in Single-Crystal Czochralski Silicon. *J. Cryst. Growth* **1995**, *154*, 47−53.

(3) Jahanmahin, O.; Kirby, D. J.; Smith, B. D.; Albright, C. A.; Gobert, Z. A.; Keating, C. D.; Fichthorn, K. A. Assembly of Gold Nanowires on Gold Nanostripe Arrays: Simulation and Experiment. *J. Phys. Chem. C* **2020**, *124*, 9559−9571.

(4) Balankura, T.; Yan, T.; Jahanmahin, O.; Narukatpichai, J.; Ng, A.; Fichthorn, K. A.; Fichthorn, K. A. Oriented Attachment Mechanism of Triangular Ag Nanoplates: A Molecular Dynamics Study. *Nanoscale Adv.* **2020**, *2*, 2265−2270.

(5) Kamon, Y.; Harima, H.; Yanase, A.; Katayama-Yoshida, H. Ultra-Fast Diffusion Mechanism of the Late 3d Transition Metal Impurities in Silicon. *Phys. B* **2001**, *308*, 391−395.

(6) Dalili, N.; Li, P.; Kupsta, M.; Liu, Q.; Ivey, D. G. In Situ TEM Study of Stability of TaRhx Diffusion Barriers Using a Novel Sample Preparation Method. *Micron* **2014**, *58*, 25−31.

(7) Shirai, K.; Michikita, T.; Katayama-Yoshida, H. Molecular Dynamics Study of Fast Diffusion of Cu in Silicon. *Jpn. J. Appl. Phys.* **2005**, *44*, 7760−7764.

(8) Buonassisi, T.; Marcus, M. A.; Istratov, A. A.; Heuer, M.; Ciszek, T. F.; Lai, B.; Cai, Z.; Weber, E. R. Analysis of Copper-Rich Precipitates

in Silicon: Chemical State, Gettering, and Impact on Multicrystalline Silicon Solar Cell Material. *J. Appl. Phys.* **2005**, *97*, No. 063503.
(9) Talapin, D. V.; Lee, J. S.; Kovalenko, M. V.; Shevchenko, E. V. Prospects of Colloidal Nanocrystals for Electronic and Optoelectronic Applications. *Chem. Rev.* **2010**, *110*, 389−458.
(10) Lee, C.; Meteer, J.; Narayanan, V.; Kan, E. C. Self-Assembly of Metal Nanocrystals on Ultrathin Oxide for Nonvolatile Memory Applications. *J. Electron. Mater.* **2005**, *34*, 1−11.
(11) Cheng, Y.-L.; Chiu, T.-J.; Wei, B.-J.; Wang, H.-J.; Wu, J.; Wang, Y.-L. Effect of Copper Barrier Dielectric Deposition Process on Characterization of Copper Interconnect. *J. Vac. Sci. Technol., B: Microelectron. Nanometer Struct.–Process., Meas., Phenom.* **2010**, *28*, 567−572.
(12) Čechal, J.; Polčák, J.; Kolíbal, M.; Bábor, P.; Šikola, T. Formation of Copper Islands on a Native SiO 2 Surface at Elevated Temperatures. *Appl. Surf. Sci.* **2010**, *256*, 3636−3641.
(13) Kershaw, S. V.; Susha, A. S.; Rogach, A. L. Narrow Bandgap Colloidal Metal Chalcogenide Quantum Dots: Synthetic Methods, Heterostructures, Assemblies, Electronic and Infrared Optical Properties. *Chem. Soc. Rev.* **2013**, *42*, 3033−3087.
(14) Guzman, D. M.; Onofrio, N.; Strachan, A. Stability and Migration of Small Copper Clusters in Amorphous Dielectrics. *J. Appl. Phys.* **2015**, *117*, No. 195702.
(15) Lindroos, J.; Fenning, D. P.; Backlund, D. J.; Verlage, E.; Gorgulla, A.; Estreicher, S. K.; Savin, H.; Buonassisi, T. Nickel: A Very Fast Diffuser in Silicon. *J. Appl. Phys.* **2013**, *113*, No. 204906.
(16) Istratov, A. A.; Flink, C.; Hieslmair, H.; Weber, E. R.; Heiser, T. Intrinsic Diffusion Coefficient of Interstitial Copper in Silicon. *Phys. Rev. Lett.* **1998**, *81*, 1243−1246.
(17) Nejatishahidein, N.; Borujeni, E. E.; Roush, D. J.; Zydney, A. L. Effectiveness of Host Cell Protein Removal Using Depth Filtration with a Filter Containing Diatomaceous Earth. *Biotechnol. Prog.* **2020**, *81*, No. e3028.
(18) Jung, S. Y.; Nejatishahidein, N.; Kim, M.; Borujeni, E. E.; Fernandez, L. C.; Roush, D. J.; Borhan, A.; Zydney, A. L. Quantitative Interpretation of Protein Breakthrough Curves in Small-Scale Depth Filter Modules for Bioprocessing. *J. Membr. Sci.* **2021**, *627*, No. 119217.
(19) Roshan, K. A.; Tang, Z.; Guan, W. High Fidelity Moving Z-Score Based Controlled Breakdown Fabrication of Solid-State Nanopore. *Nanotechnology* **2019**, *30*, No. 095502.
(20) Roshan, K. A.; Tang, Z.; Guan, W. In *False Negative and False Positive Free Nanopore Fabrication Via Adaptive Learning of the Controlled Dielectric Breakdown*, 2019 20th International Conference on Solid-State Sensors, Actuators and Microsystems and Eurosensors XXXIII, TRANSDUCERS 2019 and EUROSENSORS XXXIII; IEEE, 2019; pp 1756−1759.
(21) Xing, X.; Chau, M. L.; Roshan, K. A.; Yobas, L. In *Dielectrophoretic Cell Sorting via Sliding Cells on 3D Silicon Microelectrodes*, 2017 IEEE 30th International Conference on Micro Electro Mechanical Systems (MEMS); IEEE, 2017; pp 147−150.
(22) Van Duin, A. C. T.; Dasgupta, S.; Lorant, F.; Goddard, W. A. ReaxFF: A Reactive Force Field for Hydrocarbons. *J. Phys. Chem. A* **2001**, *105*, 9396−9409.
(23) Chenoweth, K.; Van Duin, A. C. T.; Goddard, W. A. ReaxFF Reactive Force Field for Molecular Dynamics Simulations of Hydrocarbon Oxidation. *J. Phys. Chem. A* **2008**, *112*, 1040−1053.
(24) Soria, F. A.; Zhang, W.; Van Duin, A. C. T.; Patrito, E. M. Thermal Stability of Organic Monolayers Grafted to Si(111): Insights from ReaxFF Reactive Molecular Dynamics Simulations. *ACS Appl. Mater. Interfaces* **2017**, *36*, 30969−30981.
(25) Urata, S.; Kuo, A. T.; Murofushi, H. Origin of Flexibility of Organic-Inorganic Aerogels: Insights from Atomistic Simulations. *J. Phys. Chem. C* **2018**, *35*, 20555−20563.
(26) Rajabpour, S.; Mao, Q.; Gao, Z.; Khajeh Talkhoncheh, M.; Zhu, J.; Schwab, Y.; Kowalik, M.; Li, X.; van Duin, A. C. T. Low-Temperature Carbonization of Polyacrylonitrile/Graphene Carbon Fibers: A Combined ReaxFF Molecular Dynamics and Experimental Study. *Carbon* **2021**, *174*, 345−356.
(27) Mao, Q.; Rajabpour, S.; Kowalik, M.; van Duin, A. C. T. Predicting Cost-Effective Carbon Fiber Precursors: Unraveling the Functionalities of Oxygen and Nitrogen-Containing Groups during Carbonization from ReaxFF Simulations. *Carbon* **2020**, *159*, 25−36.
(28) Zhang, L.; Kowalik, M.; Gao, Z.; Ashraf, C. M.; Rajabpour, S.; Bumgardner, C.; Schwab, Y.; Damirchi, B.; Zhu, J.; Akbarian, D.; Klett, J. W.; van Duin, A. C. T.; Li, X. Converting PBO Fibers into Carbon Fibers by Ultrafast Carbonization. *Carbon* **2020**, *159*, 432−442.
(29) Gao, Z.; Zhu, J.; Rajabpour, S.; Joshi, K.; Kowalik, M.; Croom, B.; Schwab, Y.; Zhang, L.; Bumgardner, C.; Brown, K. R.; Burden, D.; Klett, J. W.; van Duin, A. C. T.; Zhigilei, L. V.; Li, X. Graphene Reinforced Carbon Fibers. *Sci. Adv.* **2020**, *6*, No. eaaz4191.
(30) Kowalik, M.; Ashraf, C.; Damirchi, B.; Akbarian, D.; Rajabpour, S.; Van Duin, A. C. T. Atomistic Scale Analysis of the Carbonization Process for C/H/O/N-Based Polymers with the ReaxFF Reactive Force Field. *J. Phys. Chem. B* **2019**, *123*, 5357−5367.
(31) Nejat Pishkenari, H.; Yousefi, F. S.; Taghibakhshi, A. Determination of Surface Properties and Elastic Constants of FCC Metals: A Comparison among Different EAM Potentials in Thin Film and Bulk Scale. *Mater. Res. Express* **2019**, *6*, No. 015020.
(32) Kumar, G.; Van Cleve, T.; Park, J.; Van Duin, A.; Medlin, J. W.; Janik, M. J. Thermodynamics of Alkanethiol Self-Assembled Monolayer Assembly on Pd Surfaces. *Langmuir* **2018**, *34*, 6346−6357.
(33) Yuan, S.; Guo, X.; Mao, Q.; Guo, J.; van Duin, A. C. T.; Jin, Z.; Kang, R.; Guo, D. Effects of Pressure and Velocity on the Interface Friction Behavior of Diamond Utilizing ReaxFF Simulations. *Int. J. Mech. Sci.* **2021**, *191*, 1−12.
(34) Nejat Pishkenari, H.; Barzegar, M. R.; Taghibakhshi, A. Study and Simulation of Nanoparticle Translocation Through Cell Membrane. *Iran. J. Sci. Technol., Trans. Mech. Eng.* **2019**, *2017*, 1−14.
(35) Fan, F.; Huang, S.; Yang, H.; Raju, M.; Datta, D.; Shenoy, V. B.; Van Duin, A. C. T.; Zhang, S.; Zhu, T. Mechanical Properties of Amorphous LixSi Alloys: A Reactive Force Field Study. *Modell. Simul. Mater. Sci. Eng.* **2013**, *21*, 1−15.
(36) Shin, Y. K.; Gai, L.; Raman, S.; Van Duin, A. C. T. Development of a ReaxFF Reactive Force Field for the Pt-Ni Alloy Catalyst. *J. Phys. Chem. A* **2016**, *120*, 8044−8055.
(37) Chenoweth, K.; Van Duin, A. C. T.; Dasgupta, S.; Goddard, W. A. Initiation Mechanisms and Kinetics of Pyrolysis and Combustion of JP-10 Hydrocarbon Jet Fuel. *J. Phys. Chem. A* **2009**, *113*, 1740−1746.
(38) Ashraf, C.; Van Duin, A. C. T. Extension of the ReaxFF Combustion Force Field toward Syngas Combustion and Initial Oxidation Kinetics. *J. Phys. Chem. A* **2017**, *121*, 1051−1068.
(39) Liu, L.; Bai, C.; Sun, H.; Goddard, W. A. Mechanism and Kinetics for the Initial Steps of Pyrolysis and Combustion of 1,6-Dicyclopropane-2,4-Hexyne from ReaxFF Reactive Dynamics. *J. Phys. Chem. A* **2011**, *115*, 4941−4950.
(40) Hossain, M. J.; Pawar, G.; Liaw, B.; Gering, K. L.; Dufek, E. J.; Van Duin, A. C. T. Lithium-Electrolyte Solvation and Reaction in the Electrolyte of a Lithium Ion Battery: A ReaxFF Reactive Force Field Study. *J. Chem. Phys.* **2020**, *152*, 27−39.
(41) Ostadhossein, A.; Cubuk, E. D.; Tritsaris, G. A.; Kaxiras, E.; Zhang, S.; Van Duin, A. C. T. Stress Effects on the Initial Lithiation of Crystalline Silicon Nanowires: Reactive Molecular Dynamics Simulations Using ReaxFF. *Phys. Chem. Chem. Phys.* **2015**, *17*, 3832−3840.
(42) Ostadhossein, A.; Yoon, K.; van Duin, A. C. T.; Seo, J. W.; Seveno, D. Do Nickel and Iron Catalyst Nanoparticles Affect the Mechanical Strength of Carbon Nanotubes? *Extreme Mech. Lett.* **2018**, *20*, 29−37.
(43) Chepkasov, I. V.; Baidyshev, V. S.; Tsura, V. A. Molecular Dynamic Simulation of Melting Copper-Silicon Nanoparticles. *J. Phys. Conf. Ser.* **2018**, *1015*, 838−855.
(44) Nonoda, N.; Sueoka, K. Density Functional Theory Study on Stability of Fe, Cu, and Ni Atoms Near (001) Surface of Si Wafer. *ECS J. Solid State Sci. Technol.* **2019**, *8*, 573−579.
(45) Urata, S.; Yoshino, H.; Ono, M.; Miyasaka, S.; Ando, R.; Hayashi, Y. Adhesion between Copper and Amorphous Silica: A Reactive Molecular Dynamics Study. *J. Phys. Chem. C* **2018**, *122*, 28204−28214.

(46) Tersoff, J. Empirical Interatomic Potential for Carbon, with Applications to Amorphous Carbon. *Phys. Rev. Lett.* **1988**, *61*, 2879−2888.
(47) Brenner, D. W. Empirical Potential for Hydrocarbons for Use in Simulating the Chemical Vapor Deposition of Diamond Films. *Phys. Rev. B* **1990**, *46*, 9458−9466.
(48) Mortier, W. J.; Ghosh, S. K.; Shankar, S. Electronegativity Equalization Method for the Calculation of Atomic Charges in Molecules. *J. Am. Chem. Soc.* **1986**, *181*, 4315−4320.
(49) Liang, T.; Shin, Y. K.; Cheng, Y. T.; Yilmaz, D. E.; Vishnu, K. G.; Verners, O.; Zou, C.; Phillpot, S. R.; Sinnott, S. B.; Van Duin, A. C. T. Reactive Potentials for Advanced Atomistic Simulations. *Annu. Rev. Mater. Res.* **2013**, *212*, 657−682.
(50) Van Duin, A. C. T.; Strachan, A.; Stewman, S.; Zhang, Q.; Xu, X.; Goddard, W. A. ReaxFFSiO Reactive Force Field for Silicon and Silicon Oxide Systems. *J. Phys. Chem. A* **2003**, *107*, 3803−3811.
(51) Nielson, K. D.; Van Duin, A. C. T.; Oxgaard, J.; Deng, W. Q.; Goddard, W. A. Development of the ReaxFF Reactive Force Field for Describing Transition Metal Catalyzed Reactions, with Application to the Initial Stages of the Catalytic Formation of Carbon Nanotubes. *J. Phys. Chem. A* **2005**, *109*, 493−499.
(52) Senftle, T. P.; Hong, S.; Islam, M. M.; Kylasa, S. B.; Zheng, Y.; Shin, Y. K.; Junkermeier, C.; Engel-Herbert, R.; Janik, M. J.; Aktulga, H. M.; Verstraelen, T.; Grama, A.; Van Duin, A. C. T. The ReaxFF Reactive Force-Field: Development, Applications and Future Directions. *npj Comput. Mater.* **2016**, *16*, No. 15011.
(53) Fedkin, M. V.; Shin, Y. K.; Dasgupta, N.; Yeon, J.; Zhang, W.; Van Duin, D.; Van Duin, A. C. T.; Mori, K.; Fujiwara, A.; Machida, M.; Nakamura, H.; Okumura, M. Development of the ReaxFF Methodology for Electrolyte-Water Systems. *J. Phys. Chem. A* **2019**, *123*, 2125−2141.
(54) Kwon, H.; Etz, B. D.; Etz, B. D.; Montgomery, M. J.; Messerly, R.; Shabnam, S.; Vyas, S.; Van Duin, A. C. T.; McEnally, C. S.; Pfefferle, L. D.; Kim, S.; Xuan, Y. Reactive Molecular Dynamics Simulations and Quantum Chemistry Calculations to Investigate Soot-Relevant Reaction Pathways for Hexylamine Isomers. *J. Phys. Chem. A* **2020**, *10*, 5135−5141.
(55) Damirchi, B.; Radue, M.; Kanhaiya, K.; Heinz, H.; Odegard, G. M.; Van Duin, A. C. T. ReaxFF Reactive Force Field Study of Polymerization of a Polymer Matrix in a Carbon Nanotube-Composite System. *J. Phys. Chem. C* **2020**, *124*, 20488−20497.
(56) Sun, J.; Furness, J. W.; Zhang, Y. Density Functional Theory. *Math. Phys. Theor. Chem.* **2018**, *209*, 119−159.
(57) Kohn, W.; Sham, L. J. Self-Consistent Equations Including Exchange and Correlation Effects. *Phys. Rev.* **1965**, *140*, 1133−1137.
(58) Van Duin, A. C. T.; Baas, J. M. A.; Van De Graaf, B. Delft Molecular Mechanics: A New Approach to Hydrocarbon Force Fields. Inclusion of a Geometry-Dependent Charge Calculation. *J. Chem. Soc. Faraday Trans.* **1994**, *140*, 1133−1142.
(59) Pike, N. A.; Løvvik, O. M. Calculation of the Anisotropic Coefficients of Thermal Expansion: A First-Principles Approach. *Comput. Mater. Sci.* **2019**, *167*, 257−263.
(60) Kresse, G.; Hafner, J. Ab Initio Molecular Dynamics for Open-Shell Transition Metals. *Phys. Rev. B* **1993**, *48*, No. 13115.
(61) Kresse, G.; Furthmüller, J. Efficient Iterative Schemes for Ab Initio Total-Energy Calculations Using a Plane-Wave Basis Set. *Phys. Rev. B* **1996**, *501*, 173−190.
(62) Blöchl, P. E. Projector Augmented-Wave Method. *Phys. Rev. B* **1994**, *50*, 19073−19080.
(63) Perdew, J. P.; Burke, K.; Ernzerhof, M. Generalized Gradient Approximation Made Simple. *Phys. Rev. Lett.* **1996**, *78*, 1396−1403.
(64) Kim, S.-Y.; Kumar, N.; Persson, P.; Sofo, J.; van Duin, A. C. T.; Kubicki, J. D. Development of a ReaxFF Reactive Force Field for Titanium Dioxide/Water Systems. *Langmuir* **2013**, *29*, 7838−7846.
(65) Berendsen, H. J. C.; Postma, J. P. M.; Van Gunsteren, W. F.; Dinola, A.; Haak, J. R. Molecular Dynamics with Coupling to an External Bath. *J. Chem. Phys.* **1984**, *81*, 3684−3692.
(66) Singh, M.; Lara, S.; Tlali, S. Effects of Size and Shape on the Specific Heat, Melting Entropy and Enthalpy of Nanomaterials. *J. Taibah Univ. Sci.* **2017**, *11*, 922−929.
(67) Antoniammal, P.; Arivuoli, D. Size and Shape Dependence on Melting Temperature of Gallium Nitride Nanoparticles. *J. Nanomater.* **2012**, *2012*, 415797−415803.
(68) Woolard, E. W.; Einstein, A.; Furth, R.; Cowper, A. D. Investigations on the Theory of the Brownian Movement. *Am. Math. Mon.* **1928**, *35*, No. 318.
(69) Islam, M. M.; Ostadhossein, A.; Borodin, O.; Yeates, A. T.; Tipton, W. W.; Hennig, R. G.; Kumar, N.; Van Duin, A. C. T. ReaxFF Molecular Dynamics Simulations on Lithiated Sulfur Cathode Materials. *Phys. Chem. Chem. Phys.* **2015**, *17*, 3383−3393.
(70) Weber, E. R. Transition Metals in Silicon. *Appl. Phys. A* **1983**, *30*, 1−22.
(71) Claeys, C.; Simoen, E. *Metal Impurities in Silicon- and Germanium-Based Technologies: Origin, Characterization, Control, and Device Impact*; Springer Series in Materials Science; Springer International Publishing, 2018.
(72) Vatan Meidanshahi, R.; Bowden, S.; Goodnick, S. M. Electronic Structure and Localized States in Amorphous Si and Hydrogenated Amorphous Si. *Phys. Chem. Chem. Phys.* **2019**, *21*, 13248−13257.
(73) Allan, G.; Delerue, C.; Lannoo, M. Electronic Structure and Localized States in a Model Amorphous Silicon. *Phys. Rev. B* **1998**, *57*, 6933−6940.
(74) Jaque, P.; Toro-Labbé, A. Characterization of Copper Clusters through the Use of Density Functional Theory Reactivity Descriptors. *J. Chem. Phys.* **2002**, *117*, 3208−3217.
(75) Samet, H.; Tamminen, M. K. Efficient Component Labeling of Images of Arbitrary Dimension Represented by Linear Bintrees. *IEEE Trans. Pattern Anal. Mach. Intell.* **1988**, *10*, 579−586.
(76) He, L.; Ren, X.; Gao, Q.; Zhao, X.; Yao, B.; Chao, Y. The Connected-Component Labeling Problem: A Review of State-of-the-Art Algorithms. *Pattern Recognit.* **2017**, *70*, 25−43.
(77) He, L.; Chao, Y.; Suzuki, K.; Wu, K. Fast Connected-Component Labeling. *Pattern Recognit.* **2009**, *42*, 1977−1987.
(78) Samet, H. Connected Component Labeling Using Quadtrees. *J. ACM* **1981**, *28*, 487−501.
(79) Chen, T.; Xu, R.; Li, Q. Effect of Strain Rate on Tensile Strength of Defective Silicon Nanorods. *Acta Mech. Solida Sin.* **2015**, *28*, 133−144.
(80) Zhao, Y.; Xie, G.; Zhao, J.; Wang, C.; Tang, C. Modifying Mechanical Properties of Silicon Dioxide Using Porous Graphene: Molecular Dynamics Simulations. *Mater. Res. Express* **2021**, *8*, 55012−55023.
(81) Orellana, T.; Tejado, E. M.; Funke, C.; Fütterer, W.; Riepe, S.; Moller, H. J.; Pastor, J. Y. How Do Impurity Inclusions Influence the Mechanical Properties of Multicrystalline Silicon? *Int. J. Metall. Mater. Eng.* **2015**, *78*, 115−123.

https://doi.org/10.1021/acs.jpcc.1c04178
J. Phys. Chem. C 2021, 125, 19455−19466